Flame Retardant Mechanisms of Phosphorus-Containing Polyhedral Oligomeric Silsesquioxane (DOPO-POSS) in Polycarbonate Composites

Wenchao Zhang, Xiangmei Li, Rongjie Yang

National Laboratory of Flame Retardant Materials, School of Materials, Beijing Institute of Technology, Haidian District, Beijing 100081, People's Republic of China

Received 4 January 2011; accepted 8 July 2011
DOI 10.1002/app.35203
Published online 21 October 2011 in Wiley Online Library (wileyonlinelibrary.com).

ABSTRACT: The flame retardancy mechanisms of a novel polyhedral oligomeric silsesquioxane containing 9,10-dihydro-9-oxa-10-phosphaphenanthrene-10-oxide (DOPO-POSS) in polycarbonate (PC) composites are discussed. A nice flame retardancy performance of 6 wt % DOPO-POSS/PC is detected from cone calorimeter testing. The peak heat release rate and total heat released of 6 wt % DOPO-POSS/PC decrease obviously compared with that of PC. The major pyrolysis products detected from the decomposition process of PC and 6 wt % DOPO-POSS/PC are investigated by TGA coupled with Fourier transform infrared spectrometry and mass spectrum (TGA-FTIR and TGA-MS), respectively. It is confirmed that DOPO-POSS catalyzes thermal decomposition of PC, however, reduces the release of flammable volatiles during the decomposition of PC. The condensed phase products after decomposition of PC and 6 wt % DOPO-POSS/PC are investigated by FTIR, scanning electron microscopy, energy dispersive X-ray spectroscopy, and X-ray photoelectron spectroscopy characterizations. They indicated that DOPO-POSS can accelerate the formation of char during the decomposition of PC composites. © 2011 Wiley Periodicals, Inc. J Appl Polym Sci 124: 1848–1857, 2012

Key words: polycarbonate; DOPO-POSS; flame retardancy mechanisms; pyrolysis

INTRODUCTION

Bisphenol A polycarbonate (PC), one of the fast growing engineering polymers, has excellent mechanical properties and electrical properties, widely used in electrical and electronics and other fields.[1,2] For the flame retardant properties of PC, it shows a V-2 rating in the UL-94 test because PC is a naturally high charring polymer, but strict flame retardant performance is often required for electronic and electric applications, the flame retardant technologies of PC have been developed.[3–5]

Because of the environmental problems, some halogen-containing flame retardants that have high flame resistant efficiency have been forbidden gradually.[6,7] Novel silicon-containing and phosphorus-containing compounds used as flame retardants of PC have received more and more attentions owing to the environmentally friendly consideration.[8,9]

Among various aromatic phosphates, triphenyl phosphate, resorcinol bis(diphenyl phosphate), and bisphenol-A bis(diphenyl phosphate) (BDP) have achieved great commercial success.[10] Levchik et al. postulated that the primary fire-retardant action of BDP probably takes place in the condensed phase.[11,12] However, flame retardants containing phosphorus were suggested to act in the gas phase as well through flame inhibition.[13–15] 9,10-dihydro-9-oxa-10-phosphaphenanthrene-10-oxide (DOPO) is a type of cyclic phosphate with a diphenyl structure, which has high thermal stability, good oxidation resistance, and good water resistance.[16,17] Some DOPO derivatives as flame retardant for PC/ABS could increase the LOI value and char yield.[16,18] Excellent mechanical, thermal properties, and flame retardancy of DOPO derivatives/ PC composites have been reported.[19,20] The composite had an LOI value of 31.3 and a UL-94 rating V-0 when the content of DOPO-POSS was 6 wt %.[20]

Polyhedral oligomeric silsesquioxane (POSS) molecules possess a hybrid chemical composition ($RSiO_{1.5}$), which is intermediate between silica (SiO_2) and silicones (R_2SiO).[21] POSS molecules with a nano three-dimensional structure can be incorporated into almost all kinds of thermoplastic or thermosetting polymers by blending, grafting, crosslinking, or copolymerization, to improve their mechanical and thermal properties, oxidation resistance, and reduced flammability.[22,23]

Correspondence to: R. Yang (yrj@bit.edu.cn).
Contract grant sponsor: National High Technology Research and Development Program 863; contract grant number: 2007AA03Z538.

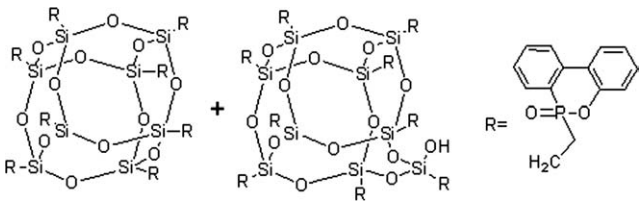

Scheme 1 Typical chemical structures of DOPO-POSS molecules.

In our previous work,[24] DOPO-containing polyhedral oligomeric silsesquioxane (DOPO-POSS) (Scheme 1) were synthesized successfully and had been introduced into PC composites. It is a novel phosphorus-containing POSS with high thermal stability. DOPO-POSS-containing PC composites exhibit enhanced mechanical properties resulting from its nanoscale dispersion in PC matrix.[20] Moreover, the thermal and flame-retardant properties of PC and PC/ABS composites with DOPO-POSS have been exposed by TGA, LOI, UL-94, and CONE test in our recent reports.[20,25] This study focuses on the flame retardant mechanisms of DOPO-POSS in PC composites.

EXPERIMENTAL

Materials

PC (Makrolon 2805) was purchased from Bayer (Shanghai). Polytetrafluoroethylene (PTFE) was obtained from Songbai Chemicals Company. DOPO-POSS was synthesized in our laboratory.[17] PC and DOPO-POSS were dried for 10 h at 120°C prior to use.

Preparation of Dopo-Poss/PC composites

PC was blended with different levels of DOPO-POSS, 0.3 wt % PTFE and small amount of antioxidants using a SJ-20 (Nanjing Giant Machinery) twin-screw extruder. The compositions of the investigated materials are shown in Table I. The blending was carried out at 275°C and a screw speed of 100 rpm, and the composites finally were cut into pellets. Samples for testing were molded by means of an injection-molding machine (HTF90 × 1, Haitian Plastics Machinery) at 275°C.

Measurements

Cone calorimeter measurements were performed at an incident radiant flux of 50 kW/m^2, according to ISO 5660 protocol, using a Fire Testing Technology apparatus with a truncated cone-shaped radiator. The specimen (100 × 100 × 3 mm^3) was measured horizontally without any grids. Typical results from cone calorimeter were reproducible within ± 10%, and the reported results are the average of these measurements.

Thermal gravimetric analysis (TGA) was performed with a Netzsch 209 F1 thermal analyzer. To detect gas species, the TGA was coupled with Fourier transform infrared spectrometry (TGA-FTIR, Nicolet 6700), and the measurements were carried out under N_2 (air) atmosphere at a heating rate of 20°C/min from 40 to 800°C. The sample weight was 10 mg for each measurement. TGA was performed at a gas flow rate of 60 mL/min.

TGA/MS characterization was performed on a Netzsch STA 449 C-QMS 403 C instrument. TGA was performed in argon of high purity at a flow rate of 25 mL/min. In the experiment, a sample weighing ~ 10 mg was heated also at 20°C/min from 35 to 800°C. Mass analysis was carried out using a spectrometer with an electron-impact ion source (70 eV); energy scanning was carried out in the range m/z 10–110 at a rate of 0.2 s^{-1} for each mass unit. The connection between TGA and MS was done by means of a quartz capillary at 200°C.

To investigate the condensed phase of the PC composites, the residues corresponding to certain temperature in TGA measurement at a heating rate of 20°C/min from 40°C. Residue after TGA test at special temperature was cooled in TGA instrument in nitrogen of high purity at a flow rate of 60 mL/min. The sample weight was 20 mg for each measurement. Then the residue was grinded and analyzed by FTIR (Nicolet 6700) directly in mode ATR.

Scanning electron microscopy (SEM) experiments were performed with a Hitachi *S*-4800 scanning electron microscope. Samples for SEM were the residue after the cone calorimeter test and sputtering the surface with gold. The C, O, Si, and P elements in the residue were verified by an energy dispersive X-ray spectroscopy (EDXS EX-350) in the SEM.

The X-ray photoelectron spectroscopy (XPS) data were obtained using a Perkin–Elmer PHI 5300 ESCA system at 250 W (12.5 kV at 20 mA) under a vacuum better than 10^{-6} Pa (10^{-8} Torr). The char residues obtained after the cone calorimeter test.

RESULTS AND DISCUSSION

Cone calorimetry

To evaluate the fire performance of 6 wt % DOPO-POSS/PC, cone calorimeter testing was carried out.

TABLE I
Composition of the Investigated Materials

Composites	PC resin (wt %)	DOPO-POSS (wt %)	PTFE (wt %)	Additives (wt %)
PC	98.7	0	0.3	1
6 wt % DOPO-POSS/PC	92.7	6	0.3	1

TABLE II
Cone Calorimeter Data for PC and 6 wt % DOPO-POSS/PC

Samples	PC	6 wt % DOPO-POSS/PC
TTI (s)	75	41
p-HRR (kW/m^2)	570	287
THR (MJ/m^2)	79.6	64.0
m-EHC (MJ/kg)	23.3	18.4
m-MLR (g/s)	0.045	0.040

Experimental results such as time to ignition (TTI), peak heat release rate (*p*-HRR), total heat released (THR), mean of effective heat of combustion (*m*-EHC), and mean of mass loss rate (*m*-MLR) obtained by cone calorimetry for the 6 wt % DOPO-POSS/PC and PC are summarized in Table II.

As shown in Table II, the TTI of 6 wt % DOPO-POSS/PC is lower than that of PC. It indicates that DOPO-POSS may accelerate the thermal decomposition of the PC matrix. Figure 1 shows the HRR during the combustion processes of PC and 6 wt % DOPO-POSS/PC. The *p*-HRR and THR of 6 wt % DOPO-POSS/PC decrease obviously. Moreover, the *m*-EHC and *m*-MLR of 6 wt % DOPO-POSS/PC reduce simultaneously compared with that for PC, and the most important is that *m*-EHC has more obvious decrease than *m*-MLR. These results indicate that fire-retardant actions of DOPO-POSS may take place in the condensed phase and gas phase simultaneously.

TGA-FTIR analysis under N_2 atmosphere

The TGA curves of PC and 6 wt % DOPO-POSS/PC created in the TGA-FTIR test are presented in Figure 2. All the onset degradation temperatures (T_{onset}) are evaluated by the temperature of 5% weight loss,

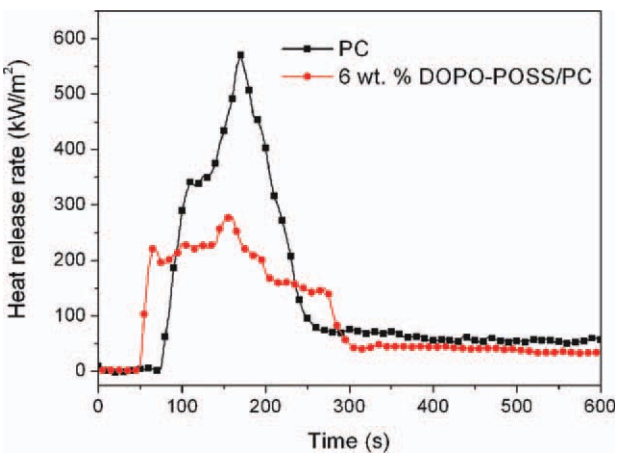

Figure 1 Heat release rate (HRR) of PC and 6 wt % DOPO-POSS/PC. [Color figure can be viewed in the online issue, which is available at wileyonlinelibrary.com.]

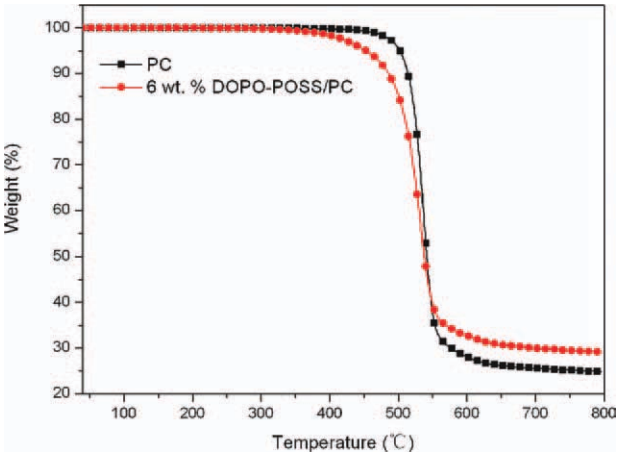

Figure 2 TGA curves of PC and 6 wt % DOPO-POSS/PC in N_2 atmosphere. [Color figure can be viewed in the online issue, which is available at wileyonlinelibrary.com.]

whereas all the T_{max} are defined as the temperature at maximum weight loss rate.

Neat PC degrades in one-step around 450–550°C under N_2 atmosphere with a T_{onset} of 502°C and a T_{max} of 543°C. Finally, the residue is 24.9% at 800°C. The T_{onset} decreases dramatically to 479°C in 6 wt % DOPO-POSS/PC, moreover, the change of T_{max} (527°C) is quite obvious compared with PC. Most importantly, more char residue (27.5%) is acquired at 800°C.

The TGA-FTIR spectra of gas phase products of PC and 6 wt % DOPO-POSS/PC at T_{max} (543°C for PC and 527°C for 6 wt % DOPO-POSS/PC) are shown in Figure 3. The assignment of the absorbance peaks are presented in Table III.

It can be seen that peaks at 3656, 3036, 3016, 2972, 2360, 1780, 1604, 1510, 1243, 1184, and 831 cm^{-1} are the characteristic absorption bands of the main

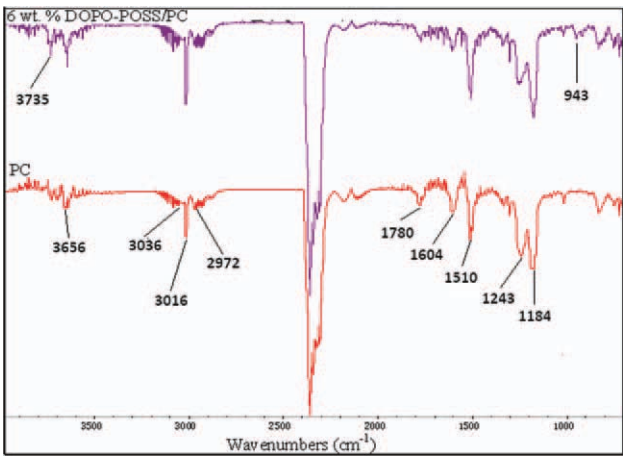

Figure 3 The FTIR spectra of pyrolysis gases of PC and 6 wt % DOPO-POSS/PC at maximum decomposition rates in N_2 atmosphere. [Color figure can be viewed in the online issue, which is available at wileyonlinelibrary.com.]

TABLE III
Assignments of Pyrolysis Gases of 6 wt % DOPO-POSS/PC at Maximum Decomposition Rates in FTIR Spectra

Wavenumber (cm^{-1})	Assignments
3656	O—H stretching vibration of C_{Ar}—OH or water
3036	C_{Ar}—H stretching vibration of styrene derivatives
3016	Methane
2972	R—CH_2—R, R—CH_3 stretching vibration of aliphatic components
2360	CO_2
1780	C=O stretching vibration of carbonyl groups
1604, 1510	aromatic rings vibration
1243, 1184	C—O stretching vibration
943	P—O stretching vibration
831	C—H deformation vibration of phenyl rings

products of the thermal decomposition of PC.[26] Although the evolving gases analysis for 6 wt % DOPO-POSS/PC is similar to that of PC, a P—O stretching vibration from volatile of DOPO-POSS was identified at 943 cm^{-1}. It implies that the DOPO-POSS might have some fire-retardant actions in the gas phase. Because PO, P, and P_2 species are likely to react with H and OH radicals to form HPO, which has been mentioned in the literature.[27]

The major pyrolysis gases detected in the decomposition process of PC and 6 wt % DOPO-POSS/PC are phenol derivatives/water (3656 cm^{-1}), styrene derivatives (3036 cm^{-1}), methane (3016 cm^{-1}), aliphatic components (2972 cm^{-1}), CO_2 (2360 cm^{-1}), and aromatic ether/ester (1243 and 1184 cm^{-1}) (Fig. 4), which corresponds well with the literature.[25]

In Figure 4, the pyrolysis products of 6 wt % DOPO-POSS/PC are detected earlier than that of PC, and this phenomenon corresponds well with the TGA curves. It indicates that DOPO-POSS may catalyze the thermal decomposition of PC matrix. The DOPO-POSS used contains acidic silanol groups that could easily hydrolyze the PC.[3] In addition, the absorbance intensity of styrene derivatives, CO_2, and aromatic ether/ester of 6 wt % DOPO-POSS/PC are lower than that of PC. The decrease of the gases evolving means the increase of char, because the volatiles such as styrene derivatives and aromatic ether/ester were from condensed-phase decomposition of the composites.[26] However, the absorbance intensity of methane for 6 wt % DOPO-POSS/PC is similar to that for PC.

TGA-FTIR analysis under air atmosphere

The TGA curves of PC and 6 wt % DOPO-POSS/PC created in the TGA-FTIR test under air atmosphere

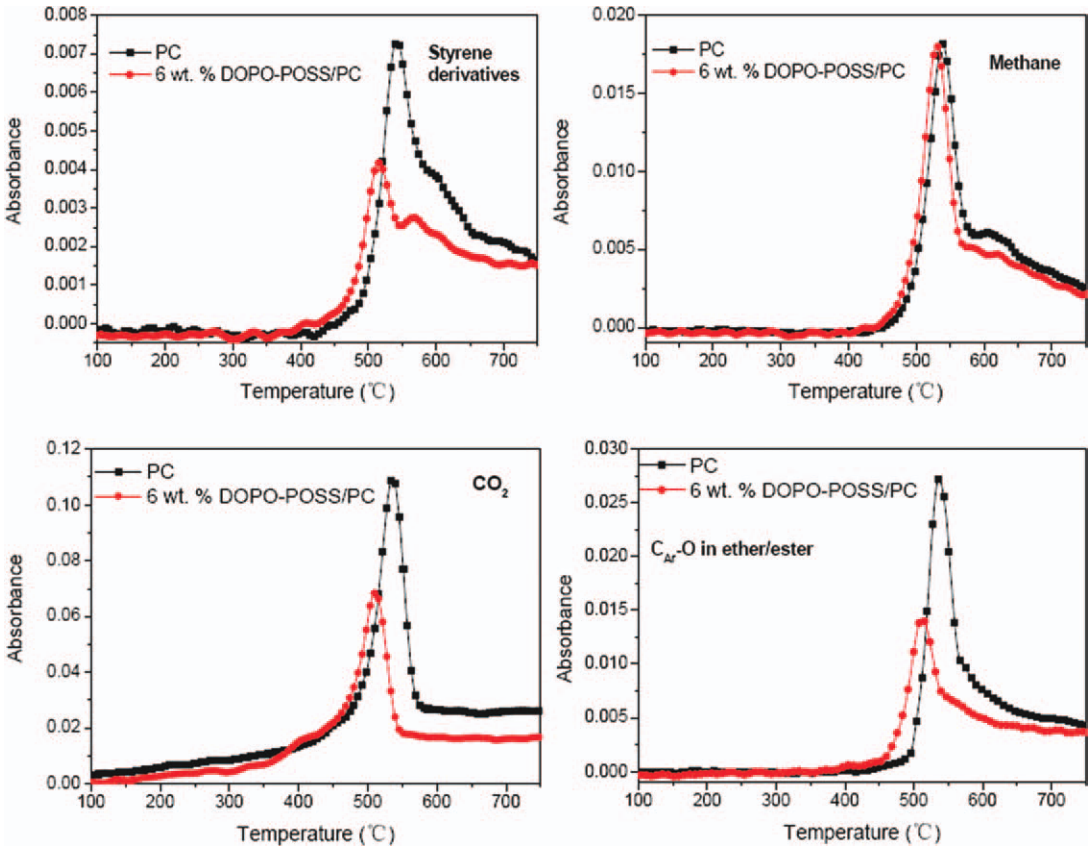

Figure 4 Product release rates of PC and 6 wt % DOPO-POSS/PC in N_2 atmosphere. [Color figure can be viewed in the online issue, which is available at wileyonlinelibrary.com.]

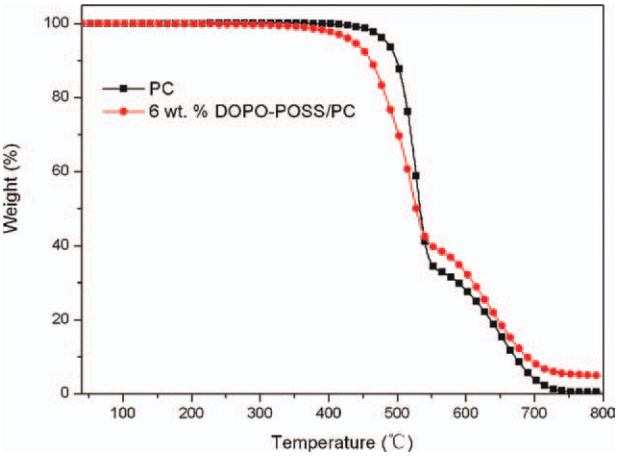

Figure 5 TGA curves of PC and 6 wt % DOPO-POSS/PC in air atmosphere. [Color figure can be viewed in the online issue, which is available at wileyonlinelibrary.com.]

are presented in Figure 5. Unlike under N_2 atmosphere, PC decomposition occurs in two distinct steps under air atmosphere. In Figure 5, PC shows a T_{onset} of 484°C, a T_{max1} of 528°C and a T_{max2} of 636°C, remaining only 0.4% char residue at 800°C. DOPO-POSS/PC of 6 wt % exhibits a similar behavior to PC under air atmosphere, whereas it features a rather reduced T_{onset} (450°C). Nevertheless, similar T_{max1} (522°C) and T_{max2} (634°C) are apparent compared with PC. The Figure 5 reveals that the interaction between PC and DOPO-POSS could reduce the thermal stability at lower temperature; however, the enhancement of the thermal stability could be found with increasing temperature. Finally, the residue is 4.9% at 800°C.

The TGA-FTIR under air was used to detect the decomposition process. The spectra of gas phase products of PC and 6 wt % DOPO-POSS/PC at T_{max1} (First step) and at T_{max2} (Second step) are shown in Figures 6 and 7.

As shown in Figure 6, the characteristic absorption bands of pyrolysis products during the decomposition of PC and 6 wt % DOPO-POSS/PC are almost similar to that in N_2 atmosphere (Fig. 3). The first step corresponds to the thermal decomposition of the PC matrix. It is reported that a series of complicated chemical reactions occur during the degradation of PC, which include the chain scission of isopropylidene linkages, hydrolysis/alcoholysis of carbonate linkages, rearrangement of carbonate linkages to form ether linkages and crosslinking reaction to form char.[28]

As shown in Figure 7, the main pyrolysis products during the second step decomposition of PC and 6 wt % DOPO-POSS/PC are CO (2180 and 2100 cm^{-1}) and CO_2 (2360 cm^{-1}). Furthermore, a spot of phenol derivatives/water, aromatic components, are also detected. These pyrolysis products are considered as

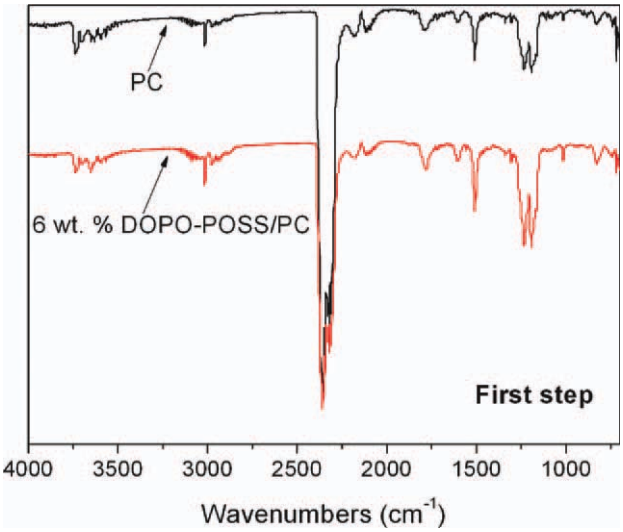

Figure 6 The FTIR spectra of pyrolysis gases of PC and 6 wt % DOPO-POSS/PC at T_{max1} in air atmosphere. [Color figure can be viewed in the online issue, which is available at wileyonlinelibrary.com.]

the thermo-oxidative decomposition of the char formed in the first step.[8,29]

In Figure 8, the pyrolysis products for 6 wt % DOPO-POSS/PC are detected earlier than that of PC, moreover, the absorbance intensity of styrene derivatives, CO_2, and aromatic ether/ester of 6 wt % DOPO-POSS/PC are lower than that of PC, which mean the increase of residue. These results are similar to that in N_2 atmosphere. It is interesting to note that the second release peaks of CO_2 and styrene derivatives are observed with the increase of temperature during the decomposition of PC and 6 wt % DOPO-POSS/PC. It is considered as the thermo-

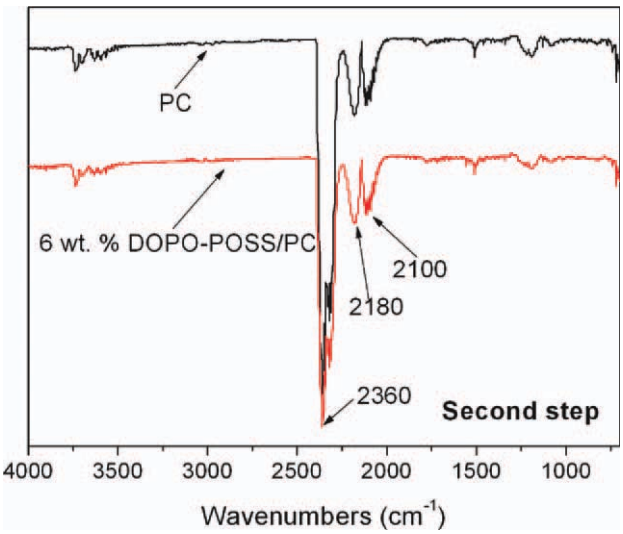

Figure 7 The FTIR spectra of pyrolysis gases of PC and 6 wt % DOPO-POSS/PC at T_{max2} in air atmosphere. [Color figure can be viewed in the online issue, which is available at wileyonlinelibrary.com.]

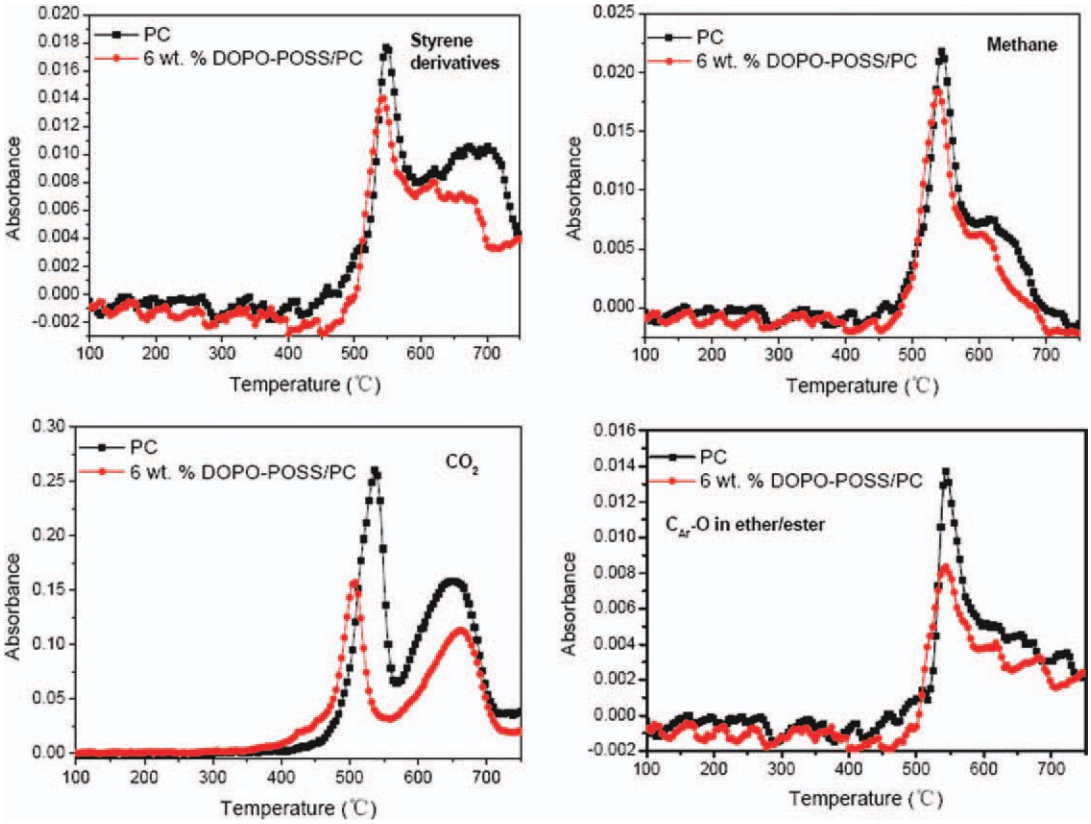

Figure 8 Product release rates of PC and 6 wt % DOPO-POSS/PC in air atmosphere. [Color figure can be viewed in the online issue, which is available at wileyonlinelibrary.com.]

oxidative decomposition of the char formed in the first step. Furthermore, the absorbance intensity of CO_2 and styrene derivatives in the second release step of 6 wt % DOPO-POSS/PC is much lower than that of PC. It implies that the char of 6 wt % DOPO-POSS/PC formed in first decomposition step has better performance insulating the underlying matrix from the oxygen and slowing down the thermal-oxidative decomposition.

TGA-MS analysis

The degradation products of the 6 wt % DOPO-POSS/PC are determined by thermogravimetry coupled to a mass spectrometer. The volatilization profiles, represented as ion current, of the fragments originating from the thermal degradation of 6 wt % DOPO-POSS/PC are shown in Figure 9. The possible structural assignments of the fragments are listed in Table IV. The mass range recorded is in 16–108 (*m/z*). The releases of methane and CO_2 during the degradation process are confirmed by the fragments at *m/z* 16 and 44. This supports the TGA-FTIR data where methane and carbon dioxide has been observed too. The signals at *m/z* 51, 65, 78, and 92, which can be assigned to benzene derivatives,[28,30] can be detected in the whole degradation process. The signals at *m/z* 94, 107, and 108 are due to phenol derivatives.[30,31] The signals of *m/z* 47 and 63 can be assigned to $OP^{+\cdot}$ and O_2P^+. All these data were supported by the TGA-FTIR analysis.

FTIR analysis

Figure 10 shows the FTIR spectra of the condensed-phase products of the PC composites at particular temperature in TGA test. The assignments of the FTIR absorption bands for 6 wt % DOPO-POSS/PC at 25°C are presented in Table V.

As shown in Figure 10, the condensed phase FTIR spectra of PC at 25°C is similar to that of 6 wt % DOPO-POSS/PC. However, at 909 cm^{-1} a small P—O—phenyl stretching vibration from DOPO-POSS is identified,[24,32] but no other additional absorption bands from DOPO-POSS is found due to the lower concentration of DOPO-POSS in comparison to PC.

In Figure 10, the FTIR spectrum of PC at 485°C is similar to that at 25°C. It means that the main structure of PC has not decomposed at 485°C. However, the spectra of the 6 wt % DOPO-POSS/PC at 485°C present a new C=C— stretching bands of aromatic rings at 1661 cm^{-1}. This result might be assigned to

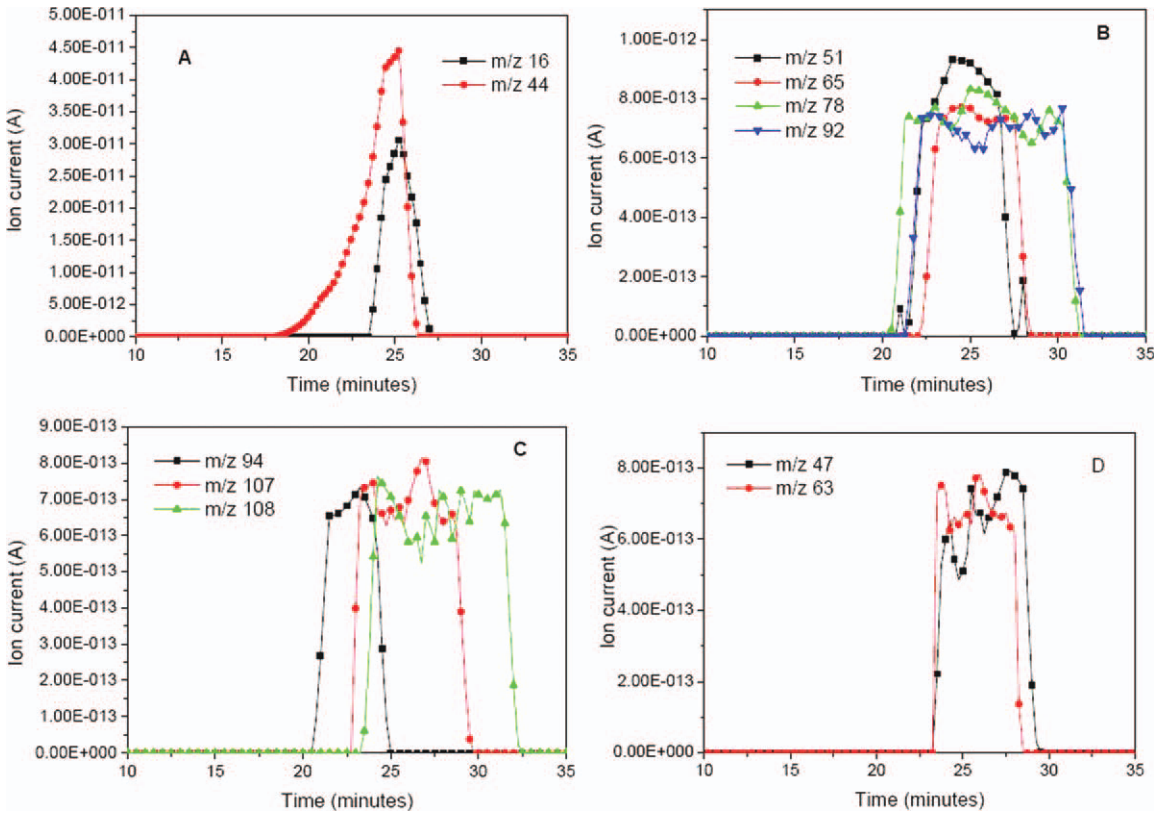

Figure 9 Ion curves for species produced from degradation of 6 wt % DOPO-POSS/PC. [Color figure can be viewed in the online issue, which is available at wileyonlinelibrary.com.]

the new aromatic structure generated by the chain scission of PC linkages[26,33] and the crosslinking reaction of decomposition products.[3] It indicates that DOPO-POSS can catalyze PC matrix decomposition. In addition, the spectra of the 6 wt % DOPO-POSS/PC at 485°C shows a new broad absorption band at 966 cm^{-1}. This new absorption band may be assigned to Si-O-phenyl stretching vibration and P-O-phenyl stretching vibration, which has been reported in some articles.[26,31]

In Figure 10, the stretching band of carbonyl groups for 6 wt % DOPO-POSS/PC is weaker than that for PC at 525°C. It indicates that the chain scission of carbonate linkages in 6 wt % DOPO-POSS/PC happened early, which corresponds well with that in the TGA-FTIR analysis section. The absorption band at 966 cm^{-1} enhances gradually and shifts to 960 cm^{-1} in 6 wt % DOPO-POSS/PC at 525°C, which means more Si—O—phenyl and P—O—phenyl structures have formed in the residue.

The FTIR spectra of the PC and 6 wt % DOPO-POSS/PC obtained at 565°C (Fig. 10) show two significant changes. The C=C stretching vibration of aromatic rings weakens obviously and splits into two absorbance bands at 1501 and 1440 cm^{-1}. These indicate some new aromatic structure generated by crosslinking reaction among decomposition products. The characteristic peaks of Si—O—phenyl and P—O—phenyl shift to 955 cm^{-1} and become to be the strongest absorbance band in the spectra, which means most part of the residue of 6 wt % DOPO-POSS/PC are Si—O—phenyl and P—O—phenyl structures. It indicates that DOPO-POSS have an obvious action on PC in the condensed-phase. The FTIR analysis of the condensed phase products of the PC composites means that the primary flame-retardant action of DOPO-POSS probably takes place in the condensed phase.

TABLE IV
Possible Structural Assignments in the Degradation of 6 wt % DOPO-POSS/PC in MS

m/z	Structures	m/z	Structures
16	CH_4	78	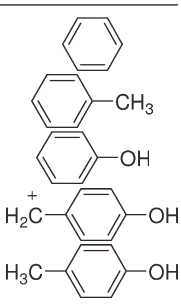
44	CO_2	92	
47	$OP^{+\cdot}$		
51		94	
63	O_2P^+	107	
65		108	

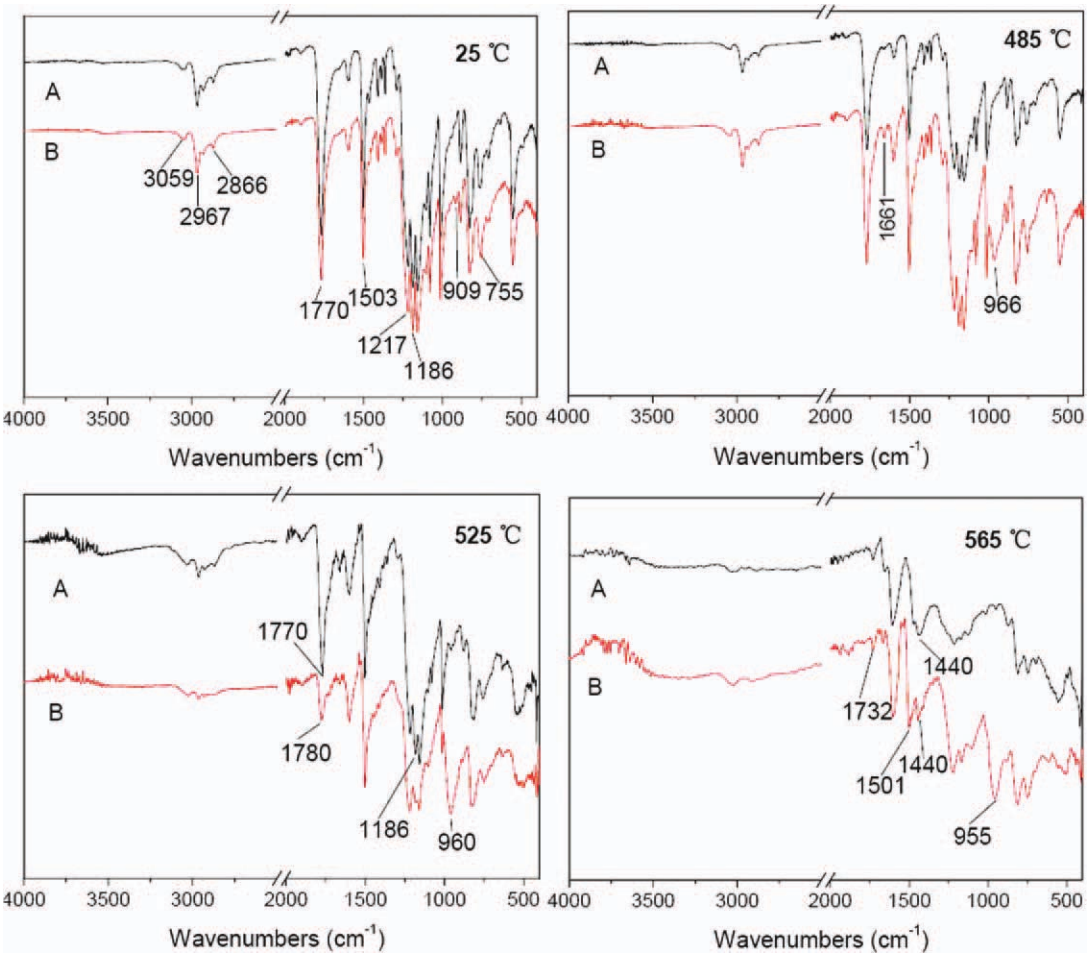

Figure 10 FTIR spectra of the condensed-phase products. (A) PC and (B) 6 wt % DOPO-POSS/PC. [Color figure can be viewed in the online issue, which is available at wileyonlinelibrary.com.]

SEM and XPS analysis

Figure 11 shows the SEM photographs obtained from exterior and interior char residues of the PC and 6 wt % DOPO-POSS/PC after the cone calorimeter tests. The exterior char of PC presents a smooth and continual char layer, and the interior char of the PC presents some holes and bubbles, which means the rapid swelling during the combustion process.

The exterior char of 6 wt % DOPO-POSS/PC sample presents a continual char layer too, however, the rough regions (I) and the smooth regions (II) can be differentiated distinctly. The EDXS spectrum of rough regions (I) and smooth regions (II) are shown in Figure 12. It indicates that the concentrations of Si and P in the rough regions (I) are higher than that in the smooth regions (II). The formation of uneven concentrations of P and Si may be a gradually process. The P and Si from the DOPO-POSS can be brought towards the surface by the pyrolysis products during combustion.[1] Then P and Si rich char would accumulate together, which separated from char of PC matrix due to the different viscosity. It can be concluded that the areas of P and Si rich would increase gradually during combustion.

To further demonstrate the enhanced barrier effect of DOPO-POSS, using XPS to analyze the char residues is a good choice. The atomic concentration

TABLE V
The Assignments of Condensed-Phase Products of 6 wt % DOPO-POSS/PC at 25°C in FTIR spectra

Wavenumber (cm^{-1})	Assignment
3059	C—H stretching vibration of aromatic rings
2967, 2929, 2866	C—H stretching vibration of aliphatic components
1770	C=O stretching vibration of carbonyl groups
1600, 1503	Aromatic rings vibration
1217, 1157	C—O stretching vibration
1186	C—C deformation vibration of isopropyl groups
909	P—O—phenyl stretching vibration
755	C—H deformation vibration of phenyl rings

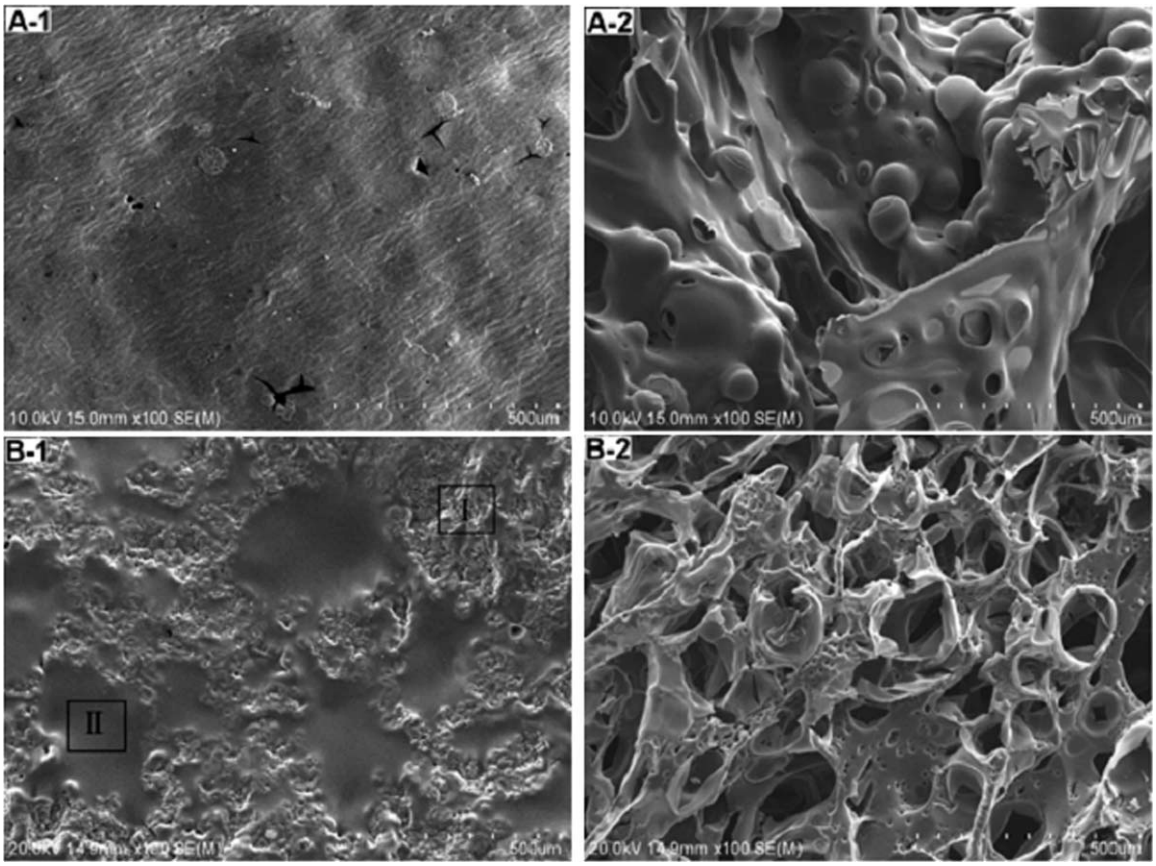

Figure 11 Residue morphologies: PC exterior (A-1), PC interior (A-2), 6 wt % DOPO-POSS/PC exterior (B-1), and 6 wt % DOPO-POSS/PC interior (B-2).

presented in Table VI is described by the percentage fraction of C, O, P, and Si atoms calculated.

It is noticed that both P and Si concentrations in the exterior char are higher than those in the interior char for 6 wt % DOPO-POSS/PC. This implies that P and Si from the DOPO-POSS would migrate towards the surface during combustion. Analogous results are obtained as reported by He et al.[1] It is reported that Si and P are helpful to form a firm char of high thermostability.[19,20] C/O ratio in these char residues are listed in Table VI. The C/O ratios in all exterior chars are almost the same. However, C/O ratio in the interior char of 6 wt % DOPO-POSS/PC is higher than that of the PC. This confirms that the formation of char could insulate the underlying matrix from the oxygen and slowing down the thermal-oxidative decomposition.

CONCLUSIONS

The flame retardant mechanisms of DOPO-POSS in PC composites have been investigated by the analysis of flame retardancy, thermal stability, pyrolysis products, and condensed-phase products of the PC

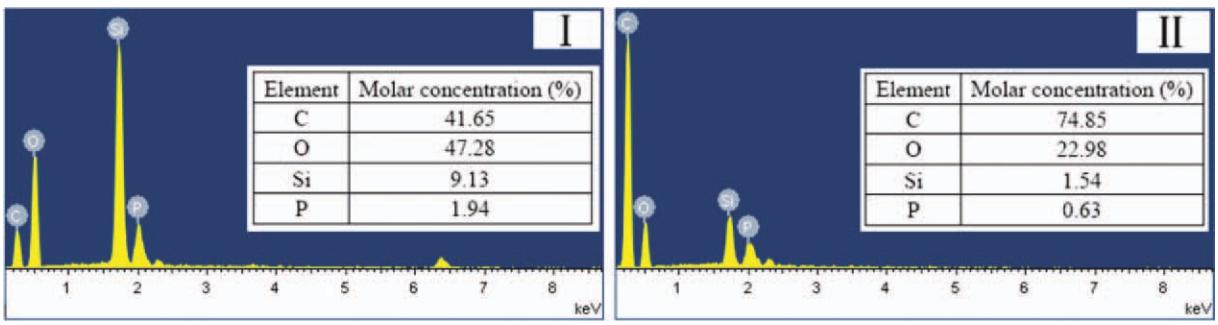

Figure 12 EDXS spectra of exterior chars of 6 wt % DOPO-POSS/PC [Fig. 11(B1)]. [Color figure can be viewed in the online issue, which is available at wileyonlinelibrary.com.]

TABLE VI
XPS Results of the Residual Char of PC and 6 wt % DOPO-POSS/PC

System	Element concentration (%)				
	C	O	Si	P	C/O[a]
PC (surface)	60.42	39.58	0	0	1.53
PC (interior)	70.98	29.02	0	0	2.45
6 wt % DOPO-POSS/PC (surface)	57.66	37.18	3.58	1.58	1.55
6 wt % DOPO-POSS/PC (interior)	75.21	22.54	1.80	0.46	3.34

[a] C/O is the ratio of carbon/oxygen atomic concentrations in the char residue.

composites. The values of *p*-HRR and THR of 6 wt % DOPO-POSS/PC obtained from cone calorimeter are effectively reduced with DOPO-POSS loading. However, the TTI is largely reduced by DOPO-POSS. The decomposition of 6 wt % DOPO-POSS/PC shows significant changes compared with PC by TGA-FTIR and TGA-MS analysis. DOPO-POSS can reduce the release of styrene derivatives, CO_2, and aromatic ether/ester during the decomposition of PC, which means the increase of char. The results of FTIR, SEM, EDXS, and XPS characterizations of the condensed-phase products from decomposition of the PC composites indicate that DOPO-POSS can participate in formation of Si—O—phenyl and P—O—phenyl crosslinking structures, which is beneficial to enhancements of the thermo-oxidative stability of the char.

References

1. He, Q. L.; Song, L.; Hu, Y.; Zhou, S. J mater Sci 2009, 44, 1308.
2. Feng, J.; Hao, J. W.; Du, J. X.; Yang, R. J. Polym Degrad Stab 2010, 95 2041.
3. Levchik, S. V.; Weil, E. D. Polym Int 2005, 54, 981.
4. Liu, S. M.; Ye, H.; Zhou, Y. S.; He, J. H.; Jiang, Z. J.; Zhao, J. Q.; Huang, X. B. Polym Degrad Stab 2006, 91, 1808.
5. Zhou, W. J.; Yang, H.; Zhou, J. J Anal Appl Pyrolysis 2007, 78, 413.
6. Chow, W. S.; Neoh, S. S. J Appl Polym Sci 2009, 114, 3967.
7. Becker, L.; Lenoir, D.; Matuschek, G.; Kettrup, A. J Anal Appl Pyrolysis 2001, 60, 55.
8. Zhou, W. J.; Yang, H. Thermochim Acta 2007, 452, 43.
9. Li, Q.; Jiang, P. K.; Wei, P. Polym Eng Sci 2006, 344–350.
10. Vothi, H.; Nguyen, C.; Lee, K.; Kim, J. Polym Degrad Stab 2010, 95, 1092.
11. Levchik, S. V.; Bright, D. A.; Moy, P.; Dashevsky, S. J Vinyl Addit Technol 2000, 6, 123.
12. Levchik, S. V.; Bright, D. A.; Alessio, G. R.; Dashevsky, S. J Vinyl Addit Technol 2001, 7, 98.
13. Braun, U.; Schartel, B. Macromol Chem Phys 2004, 205, 2185.
14. Green, J. J Fire Sci 1996, 14, 426.
15. Schartel, B.; Balabanovich, A. I.; Braun, U.; Knoll, U.; Artner, J.; Ciesielski, M.; Doring, M.; Perez, R.; Sandler, J. K. W.; Altstadt, V.; Hoffmann, T.; Pospiech, D. J Appl Polym Sci 2007, 104, 2260.
16. Zhong, H. F.; Wei, P.; Jiang, P. K.; Wang, G. L. Fire Mater 2007, 31, 411.
17. Lin, C. H.; Feng, C. C.; Hwang, T. Y. Eur Polym Mater 2007, 43, 725.
18. Zhong, H. F.; Wei, P.; Jiang, P. K.; Wu, D.; Wang, G. L. J Polym Sci Part B: Polym Phys 2007, 45, 1542.
19. Hu, Z.; Chen, L.; Zhao, B.; Luo, Y.; Wang, D.-Y.; Wang, Y.-Z. Polym Degrad Stab 2011, 96, 320
20. Zhang, W. C.; Li, X. M.; Guo, X. Y.; Yang, R. J Polym Degrad Stab 2010, 95, 2541.
21. Zhao, Y. Q.; Schiraldi, D. A. Polymer 2005, 46, 11640.
22. Zhang, W. A.; Fang, B.; Walther, A.; Müller, A. H. E. Macromolecules 2009, 42, 2563.
23. Zhang, Z. P.; Liang, G. Z.; Lu, T. L. J Appl Polym Sci 2007, 103, 2608.
24. Zhang, W. C.; Yang, R. J. J. Appl Polym Sci doi: 10.1002/app.34471.
25. Zhang, W. C.; Li, X. M.; Yang, R. J Polym Adv Technol 2011, 21, 1.
26. Perret, B.; Schartel, B. Polym Degrad Stab 2009, 94, 2194.
27. Pawlowski, K. H.; Schartel, B. Polym Int 2007, 56, 1404.
28. Jang, B. N.; Wilkie, C. A. Polym Degrad Stab 2004, 86, 419.
29. Jang, B. N.; Wilkie, C. A. Thermochim Acta 2005, 433, 1.
30. Wang, X.; Hu, Y.; Song, L.; Xing, W. Y.; Lu, H. D.; Lv, P.; Jie, G. X. Polymer 2010, 51, 2435.
31. Song, L.; He, Q. L.; Hu, Y.; Chen, H.; Liu, L. Polym Degrad Stab 2008, 93, 627.
32. Schartel, B.; Braun, U.; Balabanovich, A. I.; Artner, J.; Ciesielski, M.; Döring, M.; Perez, R. M.; Sandler, J. K. W.; Altstädt, V. Eur Polym Mater 2008, 44, 704.
33. Pawlowski, K. H.; Schartel, B.; Fichera, M. A.; Jäger, C. Thermochim Acta 2010, 498, 92.